separations

MDPI

Article

Identification of Photodegradation Products of Escitalopram in Surface Water by HPLC-MS/MS and Preliminary Characterization of Their Potential Impact on the Environment

Veronica Termopoli, Viviana Consonni, Davide Ballabio, Roberto Todeschini, Marco Orlandi and Fabio Gosetti *

Department of Earth and Environmental Sciences (DISAT), University of Milano-Bicocca, Piazza della Scienza 1, 20126 Milano, Italy

* Correspondence: fabio.gosetti@unimib.it

Abstract: The study concerns the photodegradation of the antidepressant escitalopram (ESC), the S-enantiomer of the citalopram raceme, both in ultrapure and surface water, considering the contribution of indirect photolysis through the presence of nitrate and bicarbonate. The effect of nitrate and bicarbonate concentrations was investigated by full factorial design, and only the nitrate concentration resulted in having a significant effect on the degradation. The kinetics of ESC photodegradation is the pseudo-first-order (half-life = 62.4 h in ultrapure water and 48.4 h in lake water). The generation of transformation products (TPs) was monitored through a developed and validated HPLC-MS/MS method. Fourteen TPs were identified in ultrapure water (one of them, at *m*/*z* 261, for the first time) and other two TPs at *m*/*z* 327 (found for the first time in this study) were identified only in presence of a nitrate. Several TPs were the same as those formed during the photodegradation of citalopram. The photodegradation pathway of ESC and its mechanism of degradation in water is proposed. The method was applied successfully to the analyses of surface water samples, in which a few dozen of ng L^{-1} of ESC was determined together with the presence of TP2, TP5 and TP12. Finally, a preliminary in silico evaluation of the toxicological profile and environmental behavior of TPs by computational models was carried out; two TPs (TP4 and TP10) were identified as of potential concern, as they were predicted mutagenic by Ames test model.

Keywords: escitalopram; degradation products; transformation products; HPLC-MS; mass spectrometry; photolysis; surface water

Citation: Termopoli, V.; Consonni, V.; Ballabio, D.; Todeschini, R.; Orlandi, M.; Gosetti, F. Identification of Photodegradation Products of Escitalopram in Surface Water by HPLC-MS/MS and Preliminary Characterization of Their Potential Impact on the Environment. *Separations* **2022**, *9*, 289. https://doi.org/10.3390/separations9100289

Academic Editor: Laura Dugo

Received: 8 September 2022
Accepted: 1 October 2022
Published: 5 October 2022

1. Introduction

Every year, there is a notable and constantly increasing trend in the number of drugs on the market. In particular, the category of antidepressant drugs has steadily increased due to their wider use for the treatment of depression or anxiety during and after the COVID19 pandemic [1].

The World Health Organization (WHO) has predicted that by 2030, depression could be the mental illness with the highest overall level of disability in the world [2]. Moreover, antidepressants are often used, or rather, abused, with other substances to create deadly cocktails to obtain psychotropic inhibiting effects [1].

A primary consequence of this wide use is the finding of these compounds in surface waters. Sensitive methods of analysis for many of these drugs are already available for determination at low concentrations. The concentration ranges of these drugs are extremely variable and depend on their frequency of use, varying from a few ng L^{-1} to μg L^{-1} for others [1].

However, these routine methods of analysis do not take into account the possible transformation products (TPs) that may originate in the environment by hydrolysis

reactions, solar radiation or microbial degradation [3]. As a matter of fact, the TPs can have comparable toxicity to, or sometimes be even more toxic than, the starting compound, and for this reason, it is also necessary and important to monitor them in the environment [4–7]. Only some of the analytical methods developed ad hoc for this purpose take into consideration the TPs of the starting compounds [8–12]; often these studies are restricted only to the drug metabolites, which are generally known, as pharmacokinetic studies are requisite before the compounds are placed on the market [13]. In fact, after their administration, antidepressants can undergo metabolic biotransformations that lead to the excretion of the starting compound or its metabolites, which reach water bodies (e.g., wastewater, surface, underground and drinking water), soils, and sediments through industrial, domestic, and hospital discharges [1].

Furthermore, it should be considered that these compounds, together with their TPs, are often only removed in small percentages, ranging from 18% to 33% [14], or pass almost undisturbed into surface waters, due to the inadequate treatment procedure of wastewater treatment plants (WWTPs) [15–17]. They can therefore be considered as emerging pollutants and thus increase the risk of possible toxic effects on aquatic organisms and on human health [18–22]. Furthermore, the active metabolites of these drugs can be converted back into their precursors during the treatment processes, leading to a concentration of the precursor in the effluent greater than that of the influent [23,24]. Therefore, it is important to know the degradation mechanism that can occur to better understand the fate of the drugs both in the environment and in aquatic organisms.

This study takes into consideration escitalopram (ESC), a new generation antidepressant drug with fewer side effects than usual and a drug well-tolerated by patients. ESC is a therapeutically active S-enantiomer of the citalopram raceme and belongs to the category of selective serotonin reuptake inhibitors (SSRIs). In vivo and in vitro studies have shown that its effectiveness is approximately double that of citalopram and it is therefore supplanting its use [25]. The drug is mostly metabolized in the liver, and the main metabolites are the two demethylated forms (S-demethylcitalopram and S-didemethylcitalopram), which lose the active pharmacological effect [25,26]. Furthermore, this drug has a dimethylamine group in its structure, which can lead to the formation of N-nitrosodimethylamine during the processes of potabilization by chlorination [27]. ESC and its metabolites are excreted primarily via the kidneys, with a small percentage of the drug excreted unchanged. The half-life of ESC in human plasma is 27–33 h [25,26].

The degradation studies in the literature mainly concern the citalopram rather than ESC. Some citalopram degradation products have been identified in water under UV radiation [14,28], under chlorination [14], and under TiO_2-mediated photocatalytic processes [29]. The pH effect on the citalopram photodegradation in lake waters has been investigated, showing an increase in the degradation time with increasing pH [27,28]. The presence of nitrates and dissolved organic matter (DOM) and their role in photodegradation were also considered, finding the first relevant and the second not relevant. [28]. Nitrate increases the photodegradation kinetics of citalopram, as does, albeit to a lesser extent, bicarbonate [29,30]. The citalopram oxidation with sodium hypochlorite leads to the formation of N-nitrosodimethylamine [27], while its thermal degradation and that of ESC were studied via GC-MS [31].

Since ESC is the active enantiomer of citalopram, a deep and comprehensive study of its specific transformation and accumulation in water is required, as chemical species with different abundances could be formed, and therefore there could be different toxicological effects on living organisms [32,33]. Furthermore, as a consequence of the enantiospecific biotransformation in WWTPs, it may happen that the enantiomeric pattern at the output is different from the one at the input [33].

ESC degradation was studied by forced degradation processes using different ICH-recommended stress conditions (HCl 2M at 80 °C, NaOH 0.1 M at 50 °C, H_2O_2 30%, thermal at 50 °C, photochemical in methanol solution or directly on the solid drug) [34];

whereas the identification of process impurities was carried out by HPLC-ESI-MS and NMR [35].

In this study, we want to test the natural degradation of ESC due to sunlight in conditions that are typical of temperate climates, such as that of Italy. Furthermore, since the indirect photolysis of citalopram is preponderant on the degradation kinetics [28,36], we want to systematically explore the effect of nitrate and bicarbonate concentrations and their interactions on degradation kinetics. Moreover, it is important to evaluate the (eco)toxicological and environmental behaviour of the products of the degradation process to assess their potential impact on the environment and eventually monitor those of more relevant concern. For this purpose, degradation experiments have been performed first in ultrapure water to evaluate the formation of TPs via direct photolysis, and then the effects of nitrate and bicarbonate concentrations and their interactions have been evaluated by a full factorial design. ESC TPs have been identified by a new and validated HPLC-MS/MS method that will be tested on different Italian river water samples.

2. Materials and Methods

2.1. Reagents

Escitalopram oxalate (ESC) (≥98%), sodium nitrate (>99%) and sodium bicarbonate (>99%) were purchased from Sigma-Aldrich (Milan, Italy), whereas methanol (UHPLC-MS grade), water (UHPLC-MS grade), ammonium acetate (LC-MS grade), formic acid (LC-MS grade) were acquired from Carlo Erba (Milan, Italy). Anions standard mixture (fluoride, chloride, nitrate, phosphate and sulfate) for ion chromatography analysis was purchased from ThermoFisher Scientific (Milan, Italy).

2.2. Instrumentation

A Solarbox 3000e (Co.Fo.Me.Gra, Milan, Italy) equipped with a water-cooled specimen tray, a xenon lamp and a soda-lime glass UV filter for the simulation of the outdoor exposure was used for solar irradiation experiments.

HPLC analyses were carried out by Ultimate 3000 system (ThermoFisher Scientific, Milan, Italy) equipped with an Ultimate 3000 Degasser, a quaternary pump LPG-3400SD, an Ultimate 3000 autosampler and an Ultimate 3000 column compartment. The HPLC was coupled to a triple quadrupole mass spectrometer TSQ Quantum Access Max (ThermoFisher Scientific, Milan, Italy) equipped with an electrospray ionization source (ESI). Data acquisition and reprocessing were performed by Xcalibur 2.2 software (ThermoFisher Scientific, Milan, Italy).

Ion chromatography (IC) analyses were carried out by an ICS-2000 system (ThermoFisher Scientific, Milan, Italy) equipped with anion self-regenerating suppressor 300 (ASRS 300, 4 mm) and a DS6 conductivity cell. A pH50 Violab DHS (XS Instruments, Modena, Italy) equipped with a combined glass Ag/AgCl electrode was employed for pH measurements.

2.3. Standard Solutions and Sample Collecting

The ESC standard stock solution (100.0 mg L^{-1}) was prepared in methanol and after proper dilution was used for the development and validation of the HPLC-MS/MS method. The solution was kept at −20 °C in dark glass vials. For the irradiation experiments, ESC aqueous solutions at 10.0 mg L^{-1} were freshly prepared and used in order to better simulate the natural photodegradation, avoiding the contribution of organic solvent in the degradation.

Real water samples were collected from some rivers of Northern Italy in rural areas, according to ISO 5667-6:2014 [37]. The lake water was collected near Asti (Piedmont, Italy) and used as a blank sample, according to ISO 5667-4:2016 [38]. In particular, three 1-L samplings were carried out in the center of the lake, each repeated twice, at depths of 0.5,

2.5 and 5 m using a Van Dorn bottle. The samples were placed in polyethylene bottles and kept in the dark and refrigerated at 4 °C until arrival in the laboratory, where they were mixed in equal parts, after determining that the chemical-physical parameters of the samples were very similar to each other (pH = 7.40 ± 0.02, COD = 7.2 ± 0.7). After collection, the samples were transported to the laboratory and 0.2 μm-filtered by polytetrafluoroethylene (PTFE) filters (Carlo Erba, Milan, Italy). The filtered samples were preserved in the dark at −20 °C.

2.4. Photodegradation Experiments

A twenty-eight mL cylindrical quartz cell (Hellma Italia, Milano, Italy) was filled with ESC ultrapure water solution (10.0 mg L^{-1}). The solution was magnetically stirred and underwent simulated sunlight irradiation on the water-cooled tray in the solarbox using an irradiation intensity of 600 W $m^{-2-}$and a temperature of 35 °C. The instrumental conditions were chosen on the basis of our previous knowledge of the solar average irradiation (day-night) and temperature in the period of May-September in Milan (similar to the natural sunlight irradiance at middle European latitude on sunny days). Each experiment was replicated three times. Aliquots of the solution (3 mL) were withdrawn at a prefixed time and preserved in dark glass vials at −20 °C until further HPLC/MS analysis. Before introducing and filling a new fresh ESC solution into the quartz cell, the latter was emptied and carefully cleaned. Control samples were kept in the dark for the same time as the irradiation experiments in order to highlight hydrolysis phenomena.

To test the effects of nitrate and bicarbonate concentrations on the ESC photodegradation, a 2-level full factorial design (FFD) was performed. The experimental domain includes typical concentrations of nitrate and bicarbonate in water bodies, ranging from 1.0 to 20.0 mgL^{-1} for nitrate [39] and from 1.0 to 100.0 mgL^{-1} for bicarbonate [40]. We used as the experimental response the half-life of ESC, which was derived from the kinetic constant of the degradation measured in the different experimental conditions. The experiment in the central point of the design was replicated three times to estimate the pure experimental error. All the FFD solutions were exposed to the same irradiation conditions of ultrapure water.

2.5. Chromatographic and Mass Spectrometric Conditions

The stationary phase was a Kinetex F5 column (50 mm × 3 mm, 2.6 μm) (Phenomenex, Bologna, Italy). The mobile phase was a mixture of ammonium acetate 1.0 mM in water with the addition of 0.1% formic acid (A) and ammonium acetate 1.0 mM in methanol with the addition of 0.1% formic acid (B), eluting at a flow rate 0.5 mL min^{-1} and the following gradient conditions: 0.00–0.50 min 5% B, 0.5–4.5 min 50% B, 4.6 min 100% B, 4.6–8.5 min 100% B, and 8.6 min to 12.5 min 5% B. The injection volume was 5.0 μL and the oven temperature was set at 40 °C.

ESI source works in positive ion mode with the following parameter settings: spray voltage 2.8 kV, capillary temperature 300 °C, vaporizer temperature 550 °C, sheath gas (N_2) pressure 55 arbitrary units (a.u.), auxiliary gas (N_2) pressure 5 a.u., and sweep gas (N_2) pressure 15 a.u. Tube lens offset and collision energy were optimized for ESC standard solution at 67 V and 25 V, respectively. The instrument works in selected reaction monitoring (SRM) keeping a full width at half maximum (FWHM) of about 0.7 u in each mass-resolving quadrupole (unit mass resolution), with a collision gas (Ar) pressure of 1.5 mTorr and a total cycle time of 0.72 s. The complete list of the monitored SRM transitions is reported in Table S1. In order to obtain complete MS/MS spectra information, the quantitation enhanced data-dependent scan (QED) mode was used. Once the selected SRM transition reaches an intensity threshold of 10000, the instrument automatically triggers QED, ramping the CE from 55 to 10 V.

2.6. Preconcentration by Solid-Phase Extraction (SPE) Procedure

The SPE cartridge was a C18-E (1 mL, 100 mg) from Phenomenex (Milan, Italy) and it was conditioned with 1.0 mL of methanol and 1.0 mL of ultrapure water (pH 11 for NaOH 0.01 M). After the loading of 10 mL of river water sample brought to pH 11 for NaOH, the cartridge was washed with 1.0 mL of water/methanol 85/15 (*v*/*v*) and then dried for 5 min under vacuum. The elution was carried out with 1 mL of methanol with the addition of formic acid 0.1%, evaporating to dryness with a gentle stream of nitrogen and reconstituted with 0.1 mL of the mobile phase at the initial gradient conditions (final pre-concentration factor 100×).

2.7. IC Conditions

The IC analyses were carried out using as analytical column a Dionex Ion Pac AS11 (250 × 4 mm) preceded by a Dionex Ion Pac AG11 (50 × 4 mm) guard column and, as mobile phase, a gradient elution of KOH (from 0.10 to 12.0 mM at 1.0 mL/min) obtained using an Eluent Generation Cartridge EGC III KOH). The injection volume was 20 μL.

2.8. Multivariate Data Analysis

Principal component analysis (PCA) has been used to analyse the (eco)toxicological and environmental fate properties of TPs, which were predicted by generally available internet resources. PCA is a well-known statistical method for exploratory data analysis [41]. It projects the data in a reduced hyperspace defined by principal components (PCs), which are orthogonal linear combinations of the original variables. PCA produces two main graphical outputs, the score and loading plots, where relationships among samples and variables can be analysed, respectively.

3. Results

3.1. Development and Validation of the HPLC-MS/MS Method

A simple triple quadrupole MS analyser was used to develop a sensitive HPLC/MS method (in SRM mode) for the study of ESC degradation and identification of ESC photodegradation products.

First, an MS/MS characterization of a methanol standard solution of ESC at 250 ng mL^{-1} was performed by infusion mode, increasing the collision energy in order to evaluate the weaker bonds within the molecule and obtain a significant fragmentation pattern that can be helpful for the identification of the unknown photodegradation products. The MS works in ESI PI mode, as there are nitrogen atoms prone to protonation present in the ESC chemical structure. The negative ion mode was also tested, however, but no photodegradation product was found with this type of ionization mode.

Later, the infusion into the mass spectrometer was carried out for the solutions collected at different times of the irradiation process in order to monitor the species that had formed during the photodegradation. MS/MS spectra of these compounds were acquired at different collision energies to understand the fragmentation pattern and identify for each species the two most abundant product ions indispensable for the building of typical SRM transition. In this way, the tube lens offset and the collision energy were optimized for all the formed photodegradation products (TPs) characterized by the respective SRM transitions; the values are the same than that of ESC standard solution. This pool of TPs was selected in the HPLC-MS/MS method, and later monitored during the whole photodegradation process.

In addition, the developed method also makes use of the QED mode, to obtain for each monitored transition a comprehensive MS/MS spectrum useful for the confirmation of the TP.

3.2. Validation of the HPLC-MS/MS Method

Standard solutions of ESC (LOQ, 0.01, 0.05, 0.1, 0.5, 1.0, 2.5, 10.0, 25.0, 50.0, 100, 250, 500, and 1000 ng mL^{-1}) were used to build two external calibration models with weighting factor $1/x$, reporting the ESC chromatographic peak area (quantifier transition) as dependent variable y and the standard concentration as independent variable x. The quality of both linear regression models was high, with $R^2 = 0.9999$ in the range 0.01–2.5 ng mL^{-1} and $R^2 = 0.9990$ between 2.5 and 1000 ng mL^{-1}. The ratio of the calculated to the theoretical concentrations at the fourteen concentration levels was always within the acceptable range of 92.4–116.9%.The limit of detection (LOD) and the limit of quantitation (LOQ) were calculated according to the International Council for Harmonisation of Technical Requirements for Pharmaceuticals for Human Use (ICH) as the analyte concentration giving a signal of $3.3s_B/b$ and $10s_B/b$, respectively, s_B being the blank standard deviation, equal to the residual standard deviation ($s_{y/x}$), and b the calibration model slope [42]. The obtained LOD and LOQ were 0.08 ng mL^{-1} and 0.28 ng mL^{-1}, respectively.

Seven replicates of the blank lake water sample were spiked with an ESC solution at a concentration giving an S/N ratio between 2.5 and 5 to calculate the method detection limit (MDL) as $MDL = t_{(n-1,\alpha=0.01)} \times s_d$, where $t = 3.14$ corresponds to a t-Student's value for 99% confidence level and six freedom degrees, and s_d is the standard deviation of the replicates. The method quantification limit (MQL) was defined as three times the MDL value. MDL and MQL were 0.09 and 0.28 ng mL^{-1}, respectively.

The repeatability was calculated by analysing five times the blank lake sample spiked with an ESC solution at MQL value, whereas the intermediate precision was determined by repeating the analyses for 7 consecutive days of the week ($n = 35$).

Both the repeatability and the intermediate precision gave a relative standard deviation (RSD%) of the precision of the concentrations lower than 6.0%, whereas those calculated for the retention time were lower than 0.8% and 2.6%, respectively.

The matrix effect (ME), calculated as $ME(\%) = \frac{slope_{add}}{slope_{ext}} \cdot 100 - 100$, was evaluated by comparing through a t-test (at 95% confidence level) the slopes of external calibration models ($slope_{ext}$) with those of the standard addition models ($slope_{add}$), with respect to the same linearity range. The latter models were calculated by spiking the lake water sample with the ESC standard solutions in the same concentration range as the external calibration models. Since the result of the t-test is equal to 0, therefore the $slope_{ext}$ is not significative different (at 95%) from $slope_{add}$, hence no significant ME was found.

Despite the low MQL of the method (0.28 ng mL^{-1}), a sample pre-concentration of at least 100 times was considered as being necessary, since ESC can be quantified in the surface water at very low concentration (even a few ng L^{-1}).

The recovery R was calculated as C_{obs}/C_{ref}, where C_{obs} was the concentration of ESC determined after the HPLC-MS/MS analysis, and C_{ref} was that of an ESC spiked solution. ESC solutions were prepared at 0.5, 50.0 and 500 ng mL^{-1}, to explore as much as possible the whole linearity range. They were added to a blank sample, which was submitted to the SPE procedure, replicating the analysis three times. The R values calculated for the three spiked concentration levels were (91.9 ± 2.0)%, (92.8 ± 0.5)%, and (93.3 ± 0.9)%, respectively. The R values have good reproducibility and were independent of the analyte concentration within the explored concentration range. There was no significant difference among the three obtained R values, as shown by a t-test at 95% confidence level. Therefore, the average recovery (R%) was of (92.7 ± 0.4)%.

3.3. Kinetics and Significant Factors of ESC Photodegradation

The results of the photodegradation experiments (Table 1) showed that ESC degradation kinetics was of the pseudo-first-order in all the considered conditions, whereas no evidence of ESC degradation was observed for the solution preserved in dark, confirming the poor hydrolysis reactions [29].

Table 1. Kinetics of escitalopram in different aqueous media conditions.

Photolysis Experiment	Nitrate (mg L^{-1})	Bicarbonate (mg L^{-1})	k (h^{-1})	$t_{1/2}$ (h)	R^2 *
UP Water [1]	-	-	0.0111 (±0.0008)	62.4 (±3.2)	0.9904
FFD [2]	1.0	1.0	0.0103 (±0.0005)	67.3 (±2.2)	0.9433
FFD	20.0	1.0	0.0255 (±0.0022)	27.2 (±1.6)	0.9487
FFD	1.0	100.0	0.0159 (±0.0011)	43.6 (±2.1)	0.9409
FFD	20.0	100.0	0.0478 (±0.0052)	14.5 (±1.1)	0.9632
FFD	10.0	50.0	0.0243 (±0.0023)	28.5 (±1.9)	0.9592
Lake water [3]	0.60	0.22	0.0143 (±0.0006)	48.4 (±1.5)	0.9984

* Determination coefficient of pseudo-first order kinetic model; [1] UP for ultrapure water; [2] FFD for Full Factorial Design; [3] Lake water as blank.

The degradation kinetics of ESC in ultrapure water are the slowest (half-life of approximately 2.6 days), while it increases in speed in the presence of nitrate and bicarbonate to about a 14.5 h half-life (when concentrations of both nitrate and bicarbonate are at the maximum values of the explored experimental domain), meaning that the degradation by indirect photolysis prevails over the direct photolysis mechanism.

As can be shown in the contour plot (Figure 1), the half-life of ESC photodegradation decreases about from 55 to 15 h with the increase of nitrate concentration (from 1 to 20 mg L^{-1}) and in minor extent (from 55 to 40) with the increasing of bicarbonate concentration (from 1 to 100 mg L^{-1}).

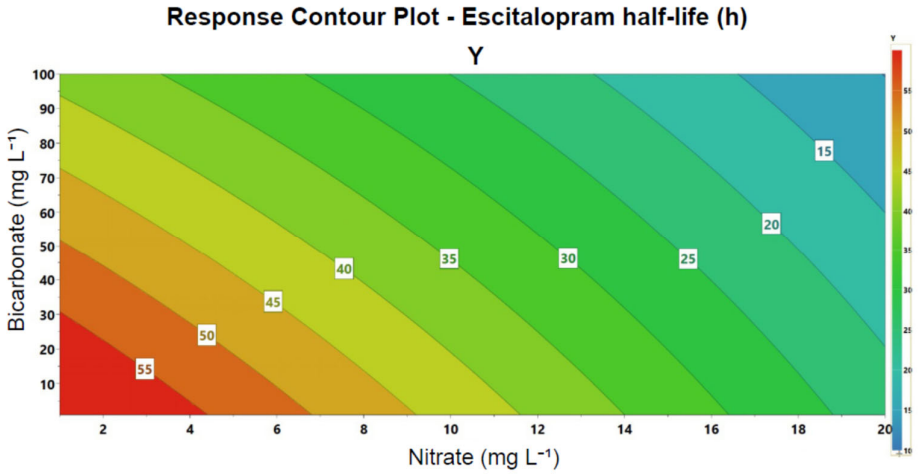

Figure 1. Contour plot of first-order FFD model: ESC half-life as a function of nitrate and bicarbonate concentrations.

The results are in agreement with other studies on citalopram degradation in water [29,30]. From the coefficients of the FFD model, calculated by multiple linear regression (R^2 = 0.8933), it was concluded that ESC photodegradation kinetics were significantly affected only by nitrate concentration (p-value < 0.02) and that the interaction effect between the two factors was not relevant. The presence of quadratic effects was excluded by performing an F-test that compared the difference between the average response of the replicated central experiments and the average response from the factorial design experiments, together with their uncertainty.

In order to evaluate the ESC photodegradation in a real water sample, the blank lake water was used. Being the concentration of nitrate and bicarbonate in lake water (0.60 ± 0.02) mg L^{-1} and (0.22 ± 0.01) mg L^{-1}, respectively, the expected half-life should be greater

than 55 h, whereas a value of 48.4 ± 0.4 was found. This observed lower half-life is probably due to the presence of DOM in the lake water at the concentration of 12.4 ± 0.11 mg L^{-1} [28]. The effect of DOM concentration was already investigated on the citalopram photodegradation and found to be much less relevant than nitrate concentration, since although DOM can promote the degradation, it can also promote its inhibition by quenching the hydroxyl radical generated by nitrate [28].

3.4. Identification of Photodegradation Products

Figure 2a shows the optimized extracted ion chromatogram of a sample of ESC in ultrapure water irradiated for 179 h. The elution time of ESC, at 4.76 min, was greater than that of all the TPs, which were labelled according to their elution order. It was evident the formation of some isomers: TP9, T12 and T16 were monitored by the same transition (341->262/109), whereas TP10 and TP13 were governed by the transition 355->292/337.

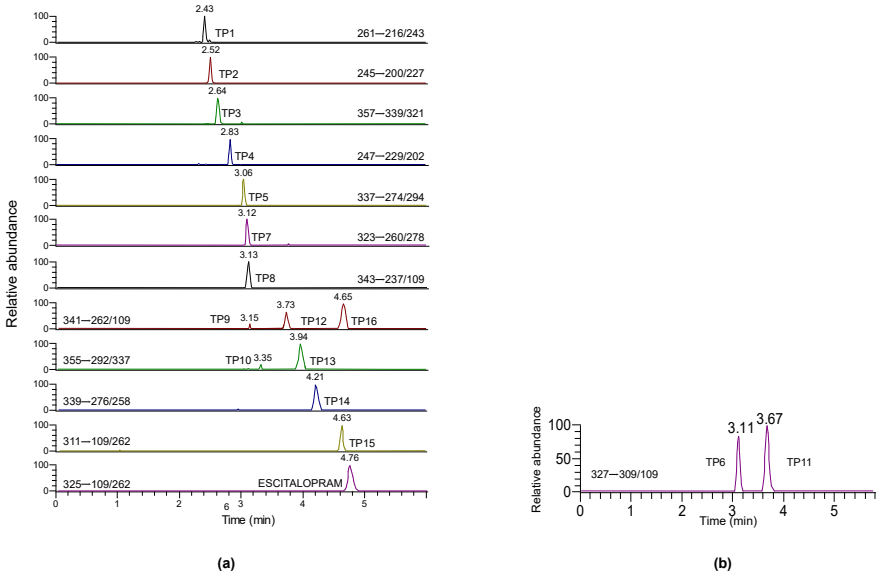

Figure 2. (**a**) Chromatographic peaks of ESC and TPs in ultrapure water after irradiation for 179 h; (**b**) additional chromatographic peaks of TPs formed in lake water for the same time of irradiation.

Considering the ESC photodegradation in ultrapure water (Figure 2a), fourteen TPs were found; among them, one (TP1) was detected for the first time. Figure 2b shows the chromatographic peaks of TP6 and TP11 (isomers monitored by the transition 327->260/278) of the lake water sample spiked with ESC at 1.0 mg L^{-1}, after the same irradiation time. Actually, TP6 and TP11 did not form in ultrapure water, but only in presence of nitrate and bicarbonate, therefore the process of indirect photolysis is supposed to be responsible for their formation [28]. As was the case for TP1, TP6 and TP11 were also identified for the first time in this study.

The starting point for the TP chemical structure elucidation was the MS/MS spectrum of the ESC, in which it was possible to identify the major product ions that could be useful to hypothesize the bonds that can most easily be broken to give rise to TPs. In fact, helpful information could really derive from the correlation between the variation of the collision energy for the ESC fragmentation and the relative abundance of the fragments in the MS/MS spectrum, according to which it was often possible to understand which fragments could be the precursors of others. Figure S1 shows the MS/MS spectrum of ESC with the chemical structures of the product ions. It can be noted that the molecule attachment points are mainly two, the alkyl chain with an alkylamine terminal and the oxygen

of the furan ring; it is therefore expected that the TPs will be formed starting from the breaking, rearrangement or modification of these parts of the molecule. The product ion with a greater *m*/*z* is at *m*/*z* 307, corresponding to a loss of water and a furan ring rearrangement. We can then find a signal at *m*/*z* 262 corresponding to dimethylamine loss. The subsequent breaking of the remaining alkyl chain and furan ring gives rise to *m*/*z* 234 and *m*/*z* 247, respectively. The base peak of the spectrum is at *m*/*z* 109, corresponding to a flurotropylium ion.

Similarly, the MS/MS characterization was made for all TPs at the irradiation time in which their intensity was maximum, and the product ions formed for each TP were correlated with those of the others, in order to find similarities in the chemical structures formed and subsequently find a common mechanism of formation. For this purpose, useful information can derive from the formation trend of the TPs during the irradiation. For example, Figure 3 shows the variation of the peak area of TP1, TP3 and TP13. It can be noted that the formation of TP3 would be correlated with that of TP13, whereas the increase of TP1 could be associated with the decrease of TP3 and TP13.

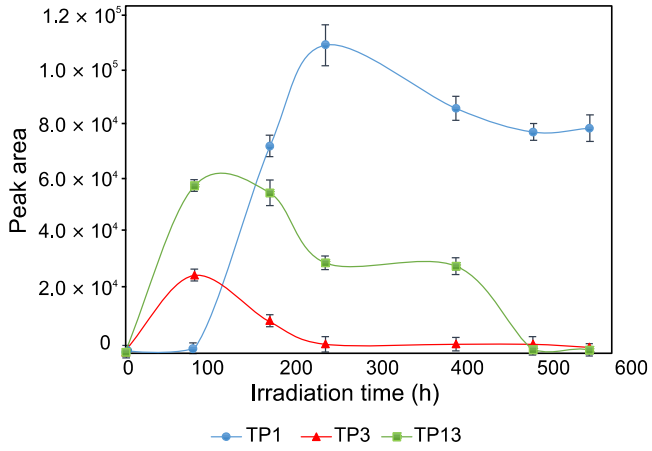

Figure 3. Time evolution of peak areas of TP1 (*m*/*z* 261), TP3 (*m*/*z* 357) and TP13 (*m*/*z* 355).

The time evolution of the other TPs is shown in Figure S2a–c, whereas Figure S2d shows the trends of all TP s with the decrease of ESC concentration in a logarithmic scale for a comprehensive view.

The chemical structures of the TPs were proposed on the basis of their quasi-molecular ion, the use of nitrogen rule, the interpretation of the MS/MS spectrum and the retention time of the species.

All identified TPs were reported in Table 2 with their retention time, the precursor ion and the most abundant product ions with their relative intensity and the references of similar TPs of citalopram.

Table 2. TPs of ESC: retention time, precursor and most abundant product ions, and the references of similar TPs already found for citalopram.

Compound Precursor Ion $[M + H]^+$	RT (min)	MS/MS Product ions (Relative Intensity, %)	Chemical Structure	Reference for Citalopram Degradation
Escitalopram 325	4.76	307 (6) 262 (33) 247 (18) 234 (30) 221 (9) 166 (9) 116 (19) 109 (100)	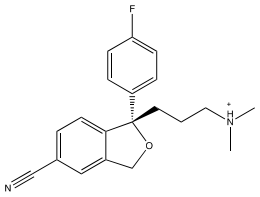	[14,29]
TP1 261	2.43	243 (100) 234 (20) 216 (38) 161 (77)	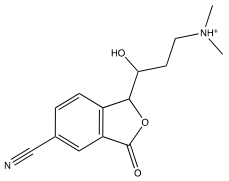	This study
TP2 245	2.52	227 (5) 200 (23) 182 (17) 158 (100) 154 (75) 141 (30)	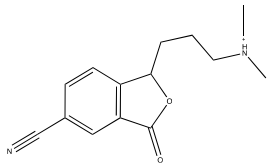	[14,28,29]
TP3 357	2.64	339 (100) 321 (8) 315 (3) 294 (5)	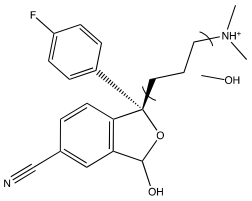	[29]
TP4 247	2.83	229 (15) 202 (5) 189 (20) 166 (100) 156 (18) 127 (40)	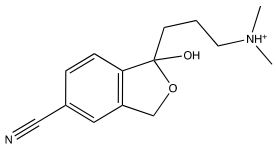	[29]
TP5 337	3.06	309 (20) 294 (100) 274 (25) 238 (60)	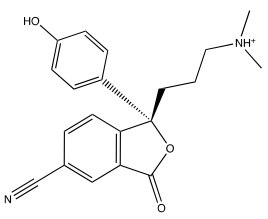	[28,29]

TP6 327	3.11	309 (15) 291 (18) 278 (20) 262 (60) 220 (5) 116 (48) 109 (100)	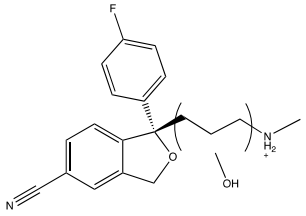	This study
TP7 323	3.12	305 (3) 287 (2) 278 (3) 260 (31) 232 (26) 166 (13) 107 (100)	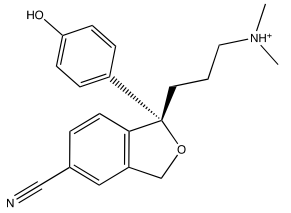	[28,29,36,43]
TP8 343	3.13	325 (35) 298 (5) 294 (45) 280 (22) 276 (30) 251 (52) 240 (100) 237 (70) 109 (60)	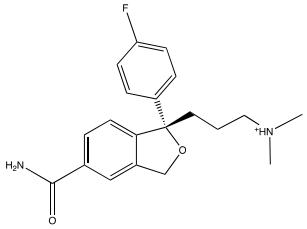	[14]
TP9 341	3.15	323 (14) 305 (17) 278 (5) 262 (72) 234 (45) 220 (18) 166 (8) 109 (100)	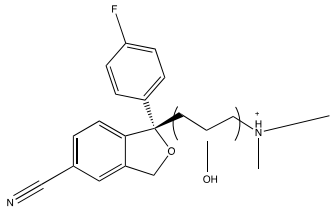	[14,29,36]
TP10 355	3.35	337 (13) 319 (100) 292 (10) 276 (49) 258 (77) 230 (25) 209 (12)	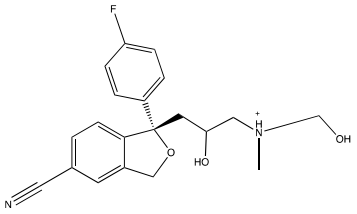	[14]
TP11 327	3.67	309 (19) 296 (8) 278 (33) 109 (100)	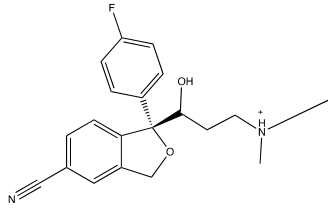	This study

TP12 341	3.73	323 (9) 296 (13) 278 (18) 240 (16) 234 (53) 221 (16) 109 (100)	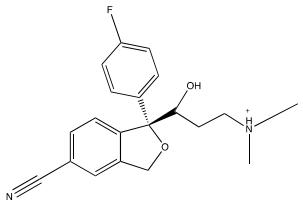	[29]
TP13 355	3.94	337 (58) 310 (4) 292 (100) 274 (13) 264 (5)	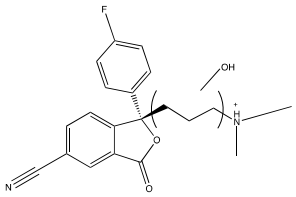	[29,36]
TP14 339	4.21	321 (5) 294 (6) 276 (100) 258 (91) 248 (19) 172 (9)	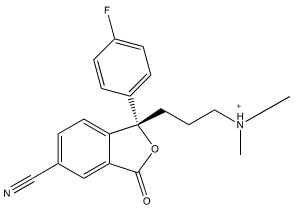	[14,28,29,36,43]
TP15 311	4.63	293 (18) 262 (52) 247 (25) 234 (33) 221 (11) 166 (10) 116 (22) 109 (100)	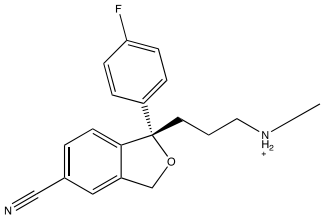	[13,14,28,30]
TP16 341	4.65	280 (6) 262 (100) 247 (11) 234 (18) 166 (7)	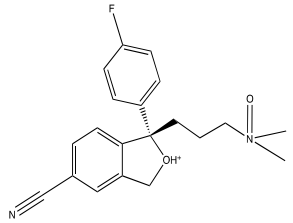	[13,14,30]

A TP7 with a signal at *m*/*z* 323, corresponding to a substitution of fluorine atom with a hydroxyl group, was already previously found for citalopram degradation [28,29,36,43]. The structure was confirmed with the presence in the MS/MS spectrum of the ion at *m*/*z* 107, corresponding to hydroxytropylium ion, instead of the characteristic fuorotropylium at *m*/*z* 109.

TP5 with an *m*/*z* signal at 337 corresponding to the oxidation on the furan ring of the TP7 according to the literature [28,29], and for successive loss of the hydroxyphenyl group can give rise to the TP2 at *m*/*z* 245 [14,28,29], which successively can undergo to hydroxylation on the aliphatic chain [14]. Unlike the process reported in the literature, the hydroxylation occurs precisely on the carbon in α position with respect to the furan ring to form TP1 at *m*/*z* 261. A confirmation of this is seen in the fragment in the MS/MS spectrum (Figure S3) at *m*/*z* 161, whose structure consists of a benzofuranone skeleton with a hydroxymethylidene substitution. In addition, the base peak at *m*/*z* 243 (loss of water) suggests that the hydroxyl group must be on the alkyl chain and the loss of water cannot

derive from furan ring (as in the MS/MS spectrum of ESC). In addition, only one loss of water is observed in the spectrum, therefore the OH position is necessarily on the α carbon close to the furan ring, preventing a subsequent loss of H_2O. The other two fragments at *m*/*z* 234 and *m*/*z* 216 correspond to a loss of the nitrile group and dimethylamine, respectively. This TP was identified and characterized for the first time in this study (Figure S3).

TP4 at *m*/*z* 247 forms after the removal of the fluorophenyl followed by a hydroxylation, as reported for citalopram degradation [29]. The ESC oxidation on the furan ring gives rise to TP14 at *m*/*z* 339 with the formation of a ketone group [14,28,29,36,43], whereas that on the amine group forms N-oxide TP16 at *m*/*z* 341, already found by Osawa et al. [14].

Two other isomers at *m*/*z* 341, namely TP9 and TP12, were identified: both derive from hydroxylation reactions on the alkyl chain, with MS/MS signals as discussed and reported by Jiménez-Holgado et al. [29]. A further hydroxylation gives to the formation of TP10 at *m*/*z* 355 and TP3 at *m*/*z* 357. In agreement with Osawa et al. [14], the MS/MS spectrum of TP10 has three fragments related to three losses of water, one of them much intense at *m*/*z* 319 attributed to the hydroxylation of the methyl group of the tertiary amine. TP3 was already found by Jiménez-Holgado et al. [29] for citalopram degradation and its subsequent oxidation on the furan ring can give origin to TP13, an isomer of TP10. TP13 could be also derived from the hydroxylation of TP14 [29], and for further loss of the fluorophenyl moiety could form TP1. Nitrile hydrolysis of ESC can give TP8 at *m*/*z* 343, previously found only by Osawa et al. [14] for citalopram degradation and confirmed by the loss of CHNO from *m*/*z* 280 to *m*/*z* 237 and from *m*/*z* 294 to *m*/*z* 251.

TP15 at *m*/*z* 311 corresponds to the N-demethylation of ESC, confirmed in the MS/MS spectrum by the presence of the signal at *m*/*z* 262 formed by a loss of NH_2CH_3 from *m*/*z* 293 [14]. A further hydroxylation gives to the formation of two isomers, identified for the first time, at *m*/*z* 327.

The MS/MS spectrum of TP6 (Figure S4) shows two successive losses of water (*m*/*z* 309 and *m*/*z* 291) suggesting the presence of OH on the alkyl chain, as explained for TP9, the elimination of NH_2CH_3 to form *m*/*z* 278 from *m*/*z* 309, the signal at *m*/*z* 109 attributed to fluorotropylium and *m*/*z* at 262, already found in the MS/MS spectrum of ESC (Figure S1).

The other isomer of TP6 is TP11, in which, similar to the TP1 discussed above, the OH position on the alkyl chain is forced to the carbon in α position close to the furan ring. In the MS/MS spectrum, only a loss of water is present (from *m*/*z* 327 to *m*/*z* 309), whereas the loss of water on the furan ring is hindered. The elimination of NH_2CH_3 corresponds to the signal at *m*/*z* 296, from which is formed *m*/*z* at 278 from the loss of water (Figure S5).

Overall, the photodegradation mechanism of ESC consists of different types of reactions (Figure 4), the main one being hydroxylation (TP9, TP12) or di-hydroxylation, both on the alkyl chain (TP10) and the furan ring (TP3), which can be followed by a subsequent oxidation step of the ring (TP13) and loss of fluorophenyl (TP1).

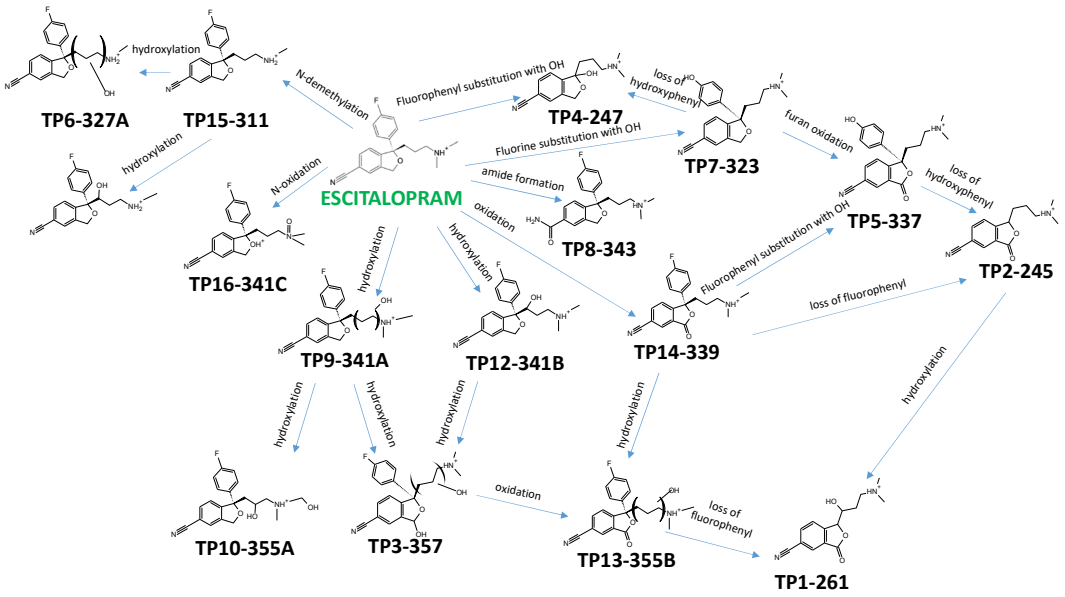

Figure 4. Proposed mechanism of reactions involved in the ESC photodegradation.

The hydroxylation reaction can also follow N-demethylation (TP15) to give rise to the remaining N-demethylation and hydroxylation (TP6) or a simple hydroxylation (TP11). N-oxidation instead leads to the formation of TP16, while the oxidation of the furan ring to TP14, from which TP5 and TP2 can originate by substitution of the fluorophenyl with OH and loss of the fluorophenyl itself, respectively. Another way to form TP5 is by the oxidation of the furan ring starting from TP7, which originates both directly from the loss of fluorophenyl of the ESC molecule, and by loss of hydroxyphenyl from TP4 formed by fluorophenyl substitution of ESC. Finally, the formation of amide gives rise to TP8.

Considering the TPs that have lost the fluorine atom (TP1, TP2, TP4, TP5 and TP7), it can be seen in Figure 5a that TP5 gives the most intense signal reaching the maximum concentration after around 100 h of irradiation, while the peak areas of the other TPs are significantly smaller and their maxima are shifted to around 200 h. The formation of fluoride ion (Figure 5b) was monitored and it can be seen that it grows up to about 100 h and then remains almost constant until the end of the irradiation time, demonstrating that the greatest contribution to its formation is due to TP5.

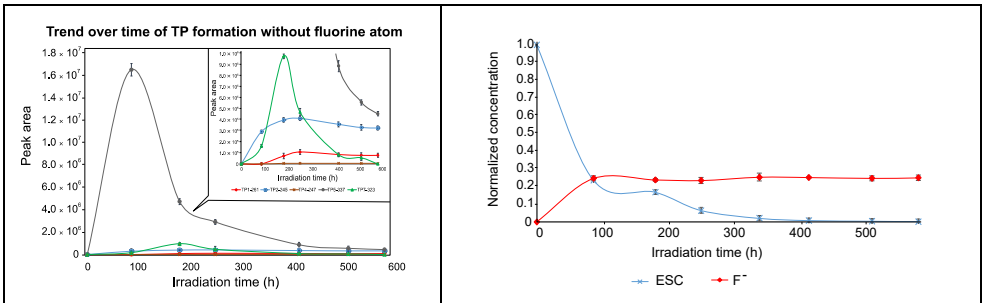

Figure 5. Time evolution of (**a**) peak areas of TPs that have lost the fluorine atom (TP1 at *m*/*z* 261, TP2 at *m*/*z* 245, TP4 at *m*/*z* 247, TP5 at *m*/*z* 337 and TP7 at *m*/*z* 323) with a zoom-section on the smallest TP peak areas, and (**b**) the related fluoride formation.

3.5. River Water Analysis

The method developed and validated was successfully applied to the analysis of five river water samples after the pre-concentration step to search for the presence of ESC and any TPs (Table 3). ESC was determined at the concentration of a few tens of ng L^{-1} in three out of five rivers, while in two of these three rivers, only three out of sixteen of the TPs, TP2, TP5 and TP12, were identified, while in the river Tanaro, only TP5 was identified.

Table 3. Quantification data in the real samples (n.d. for not detected).

Sample	ESC (ng/L)	TP2-245	TP5-337	TP12-341b
Adda river	45.8 (± 0.6)	detect	detect	detect
Po river	39.8 ± (1.4)	detect	detect	detect
Serio river	n.d.	n.d.	n.d.	n.d.
Sesia river	n.d.	n.d.	n.d.	n.d.
Tanaro river	12.5 ± (0.8)	n.d.	detect	n.d.

3.6. Toxicity Assessment of TPs

Toxicity and environmental impact of TPs were preliminarily evaluated in silico by quantitative structure-activity relationships (QSARs) and read-across models implemented in the free available internet resources VEGA [44] and T.E.S.T [45]. In particular, from the simplified molecular input line entry system (SMILES) notations [46] of ESC and its TPs, we obtained estimates of acute aquatic toxicity on fish (Fathead minnow (LC_{50}-96 h)), *Daphnia magna* (LC_{50}-48 h), *Tetrahymena pyriformis* (IGC_{50}-48 h) and acute oral toxicity on rat (LD_{50}) by the consensus method of T.E.S.T. software relaxing the fragment constraint. The VEGA platform was used to predict mutagenicity by the consensus model on Ames test, developmental toxicity by CAESAR model, bioaccumulation by Arnot-Gobas BCF model, ready biodegradability, and persistence in water, sediment and soil by IRFMN models. Predicted values of the endpoints were collected in Table S2 and investigated by principal component analysis (PCA). Figure 6 shows the similar relationships among ESC and TPs in the orthogonal space of the first two principal components (PCs), which explain 60% of the total data variance. In the score plot, TPs mainly clustered in two groups, with positive and negative scores on PC2. All variables exhibit negative loadings on PC2, while PC1 differentiates Ames and the majority of toxicities (positive loadings) versus bioconcentration and persistence in water (negative loadings). In general, most of the TPs exhibit a similar toxicological profile and environmental behaviour to ESC; only TP4 and TP10 emerge as different since, unlike ESC and the other TPs, they were predicted positive to Ames mutagenicity test. According to the Globally Harmonized System (GHS) of classification and labelling of chemicals [47], only with a few exceptions, ESC and TPs were generally labelled as being moderately toxic for aquatic environment of category 2 ($1\,mg/L < LC50 \leq 10\,mg/L$) or 3 ($10\,mg/L < LC50 \leq 100\,mg/L$). Also considering the acute toxicity on rat by oral ingestion, they were labelled as moderately toxic of category 2 ($300\,mg/kg < LD50 \leq 2000\,mg/kg$); moreover, all of the chemicals were predicted as potential interferents for normal development of humans or animals and non-ready biodegradable but with a low potential of bioaccumulation (logBCF < 3.3 according to REACH regulation EC No 1907/2006) and, accordingly, a low persistence in aquatic and terrestrial environments.

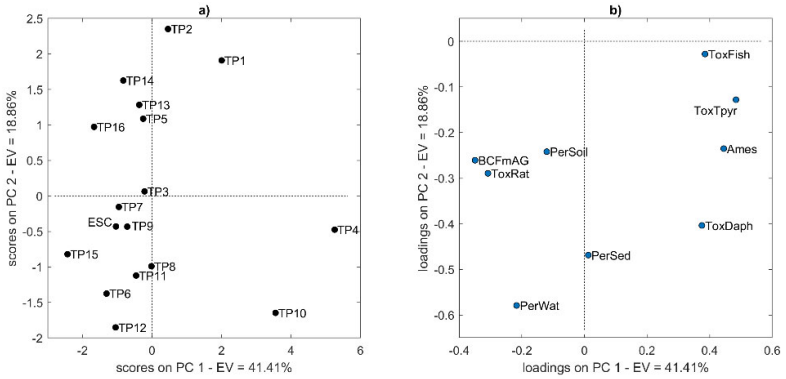

Figure 6. Graphical results of principal component analysis (PCA) of the toxicological and environmental fate endpoints for ESC and its detected TPs: (**a**) score plot and (**b**) loading plot of the first two principal components (PCs). The variable labels in the loading plot (**b**) are: acute toxicity on fish (ToxFish), Daphnia magna LC50 (ToxDaph), T. pyriformis IGC50 (ToxTpyr), oral toxicity on rat LD50 (ToxRat), mutagenicity by Ames test (Ames), log bioconcentration factor (BCFmAG), water persistence (PerWat), sediment persistence (PerSed), and soil persistence (PerSoil). Further details on variables are given in the supplementary material (Table S2).

4. Conclusions

ESC photodegraded by exposure to sunlight in aqueous solution by direct photolysis with a half-life of about 2.6 days, kinetics that increased in the presence of nitrates. The formation of 14 TPs were observed in ultrapure water and another two TPs in surface water, whose chemical structures were elucidated and toxicity evaluated by in silico simulation, which appears only in two of the TPs (TP4 and TP10) to be greater than that of ESC. Most ESC TPs are the same as those from citalopram, identified in part in other studies [14,28,29,36,43], but three new TPs can be attributed only to ESC, TP1 at *m*/*z* 261, formed also in ultrapure water, and the two isomers TP6 and TP11 at *m*/*z* 327, formed only in presence of nitrate. The mechanism of degradation involves similar reactions to citalopram degradation [14,28,29,36,43]. The results of this study will be significant in updating current knowledge on the identification of ESC TPs and may be useful for implementing micropollutant monitoring in water systems.

Supplementary Materials: The following supporting information can be downloaded at: https://www.mdpi.com/article/10.3390/separations9100289/s1, Table S1: Selected Reaction Monitoring transitions of the HPLC-MS/MS method for ESC and TPs monitoring; Table S2: In silico prediction of ecotoxicity, mutagenicity, bioaccumulation and persistence of ESC and its TPs by VEGA [1] and T.E.S.T. [2] software; Table S3: Results of matrix effect evaluation; Figure S1: MS/MS spectrum of ESC with the chemical structures of the product ions; Figure S2: Time evolution of the peak areas of TPs formed during the ESC photodegradation; Figure S3: MS/MS spectrum of TP1 at *m*/*z* 261 with the chemical structures of the product ions; Figure S4: MS/MS spectrum of TP6 at *m*/*z* 327 with the chemical structures of the product ions; Figure S5: MS/MS spectrum of TP11 at *m*/*z* 327 with the chemical structures of the product ions.

Author Contributions: Conceptualization, F.G., V.C. and V.T.; methodology, F.G., V.C. and V.T.; validation, F.G. and V.T.; formal analysis, D.B., F.G., R.T., V.C. and V.T.; investigation, F.G. and V.T.; resources, F.G. and M.O.; data curation, D.B., R.T. and V.C.; writing—original draft preparation, F.G.; writing—review and editing, D.B., F.G., M.O., R.T., V.C. and V.T.; visualization, F.G.; supervision, F.G.; project administration, F.G. All authors have read and agreed to the published version of the manuscript.

Funding: This study was financially supported by Milano-Bicocca University Fund-Departmental Fee 2019-ATE-0282.

Institutional Review Board Statement: Not applicable.

Informed Consent Statement: Not applicable.

Data Availability Statement: Not applicable.

Conflicts of Interest: The authors declare no conflicts of interest.

References

1. Diaz-Camal, N.; Cardoso-Vera, J.D.; Islas-Flores, H.; Gómez-Oliván, L.M.; Mejía-García, A. Consumption and occurrence of antidepressants (SSRIs) in pre- and post-COVID-19 pandemic, their environmental impact and innovative removal methods: A review. *Sci. Total Environ*. **2022**, *829*, 154656. http://dx.doi.org/10.1016/j.scitotenv.2022.154656.
2. Sindu, P. Management of depression with behavior therapy. *Curr. Res. Behav. Sci.* **2020**, *1*, 100001. https://doi.org/10.1016/j.crbeha.2020.100001.
3. Bavumiragira, J.P.; Ge, J.; Yin, H. Fate and transport of pharmaceuticals in water systems: A processes review. *Sci. Total Environ*. **2022**, *823*, 153635. https://dx.doi.org/10.1016/j.scitotenv.2022.153635.
4. Gosetti, F.; Chiuminatto, U.; Mazzucco, E.; Mastroianni, R.; Bolfi, B.; Marengo, E. Ultra-high performance liquid chromatography tandem high-resolution mass spectrometry study of tricyclazole photodegradation products in water. *Environ. Sci. Pollut. Res.* **2015**, *22*, 8288–8295. https://dx.doi.org/10.1007/s11356-014-3983-4.
5. Gosetti, F.; Bolfi, B.; Chiuminatto, U.; Manfredi, M.; Robotti, E.; Marengo, E. Photodegradation of the pure and formulated alpha-cypermethrin insecticide gives different products. *Environ. Chem. Lett.* **2018**, *16*, 581–590. https://doi.org/10.1007/s10311-017-0685-4.
6. Bottaro, M.; Frascarolo, P.; Gosetti, F.; Mazzucco, E.; Gianotti, V.; Polati, S.; Pollici, E.; Piacentini, L.; Pavese, G.; Gennaro, M.C. Hydrolytic and Photoinduced Degradation of Tribenuron Methyl Studied by HPLC-DAD-MS/MS. *J. Am. Soc. Mass Spectrom.* **2008**, *19*, 1221–1229. https://dx.doi.org/doi:10.1016/j.jasms.2008.05.009.
7. Gosetti, F.; Chiuminatto, U.; Zampieri, D.; Mazzucco, E.; Marengo, E.; Gennaro, M.C. A new on-line solid phase extraction high performance liquid chromatography tandem mass spectrometry method to study the sun light photodegradation of mono-chloroanilines in river water. *J. Chromatogr. A* **2010**, *1217*, 3427–3434. https://dx.doi.org/10.1016/j.chroma.2010.02.080.
8. Gosetti, F.; Belay, M.H.; Marengo, E.; Robotti E. Development and validation of a UHPLC-MS/MS method for the identification of irinotecan photodegradation products in water samples. *Environ. Pollut.* ***2020***, *256*, 113370, https://doi.org/10.1016/j.envpol.2019.113370.
9. Calza, P.; Jiménez-Holgado, C.; Coha, M.; Chrimatopoulos, C.; Dal Bello F.; Medana, C.; Sakkas, V. Study of the photoinduced transformations of sertraline in aqueous media. *Sci. Total Environ.* **2021**, *756*, 143805, https://doi.org/10.1016/j.scitotenv.2020.143805.
10. Gornik, T.; Carena, L.; Kosjek, T.; Vione, D. Phototransformation study of the antidepressant paroxetine in surface waters. *Sci. Total Environ.* **2021**, *774*, 145380. https://doi.org/10.1016/j.scitotenv.2021.145380.
11. Gros, M., Williams, M., Llorca, M., Rodriguez-Mozaz, S.; Barceló, D.; Kookana, R.S. Photolysis of the antidepressants amisulpride and desipramine in wastewaters: Identification of transformation products formed and their fate. *Sci. Total Environ.* **2015**, *530–531*, 434–444. https://dx.doi.org/10.1016/j.scitotenv.2015.05.135.
12. Metcalfe, C.D.; Chu, S.; Judt, C.; Li, H.; Oakes, K.D.; Servos, M.R.; Andrews, D.M. Antidepressants and their metabolites in municipal wastewater, and downstream exposure in an urban watershed. *Environ. Toxicol. Chem.* **2010**, *29*, 79–89. https://dx.doi.org/10.1002/etc.27.
13. Hu, Z.; Li, J.; Xiao, A.; Zheng, J.; Guan, S.; Guo, J.; Huang, M. Development and validation of UHPLC-MS/MS method for simultaneous quantification of escitalopram and its major metabolites in human plasma and its application in depressed patients. *J. Pharm. Biomed. Anal.* **2022**, *217*, 114810. https://doi.org/10.1016/j.jpba.2022.114810.
14. Osawa, R.A.; Carvalho, A.P.; Monteiro, O.C.; Oliveira, M.C.; Florêncio, M.H. Transformation products of citalopram: Identification, wastewater analysis and in silico toxicological assessment. *Chemosphere* **2019**, *217*, 858–868. https://doi.org/10.1016/j.chemosphere.2018.11.027.
15. Gornik, T.; Shinde, S.; Lamovsek, L.; Klobar, M.; Heat. E.; Sellergren, B.; Kosjek, T. Molecularly Imprinted Polymers for the Removal of Antide-Pressants from Contaminated Wastewater. *Polymers* **2021**, *13*, 120. https://doi.org/10.3390/polym13010120.
16. Rejek, M.; Grzechulska-Damszel, J. Degradation of sertraline in water by suspended and supported TiO_2. *Pol. J. Chem. Technol.* **2018**, *20*, 107–112. https://doi.org/10.2478/pjct-2018-0030.
17. Verlicchi, P; Aukidy, M.A.; Zambello, E. Occurrence of pharmaceutical compounds in urban wastewater: Removal, mass load and environmental risk after a secondary treatment—A review. *Sci. Total Environ*. **2012**, *429*, 123–155. https://doi:10.1016/j.scitotenv.2012.04.028.
18. Pivetta, R.C.; Rodrigues-Silva, C.; Ribeiro, A.R.; Rath S. Tracking the occurrence of psychotropic pharmaceuticals in Brazilian wastewater treatment plants and surface water, with assessment of environmental risks. *Sci. Total Environ*. **2020**, *727*, 138661. https://doi.org/10.1016/j.scitotenv.2020.138661.
19. Duan, S.; Fu, Y.; Dong, S.; Ma, Y.; Meng, H.; Guo, R.; Chen, J.; Liu, Y.; Li, Y. Psychoactive drugs citalopram and mirtazapine caused oxidative stress and damage of feeding behavior in *Daphnia magna*. *Ecotoxicol. Environ. Saf.* **2022**, *230*, 113147. https://doi.org/10.1016/j.ecoenv.2021.113147.

20. Ma, Y.; Xu, D.; Li, C.; Wei, S.; Guo, R.; Li, Y.; Chen, J.; Liu, Y. Combined toxicity and toxicity persistence of antidepressants citalopram and mirtazapine to zooplankton *Daphnia magna*. *Environ. Sci. Pollut. Res.* **2022**, https://doi.org/10.1007/s11356-022-20203-3.
21. Yang, H.; Lu, G.; Yan, Z.; Liu, J.; Dong, H. Influence of suspended sediment characteristics on the bioaccumulation and biological effects of citalopram in *Daphnia magna*. *Chemosphere* **2018**, *207*, 293–302. https://doi.org/10.1016/j.chemosphere.2018.05.091.
22. Fong, P.P.; Hoy, C.M. Antidepressants (venlafaxine and citalopram) cause foot detachment from the substrate in freshwater snails at environmentally relevant concentrations. *Mar. Freshw. Behav. Physiol.* **2012**, *45*, 145–153. https://doi.org/10.1080/10236244.2012.690579.
23. Calisto, V.; Esteves, V.I. Psychiatric pharmaceuticals in the environment. *Chemosphere* **2009**, *77*, 1257–1274. https://doi.org/10.1016/j.chemosphere.2009.09.021.
24. Subedi, B.; Kannan, K. Occurrence and fate of select psychoactive pharmaceuticals and antihypertensives in two wastewater treatment plants in New York State, USA. *Sci. Total Environ.* **2015**, *514*, 273–280. https://doi.org/10.1016/j.scitotenv.2015.01.098.
25. Dhillon, S.; Scott, L.J.; PLoSker, G.L. Escitalopram. A Review of its Use in the Management of Anxiety Disorders. *CNS Drugs* **2003**, *17*, 343–362. https://doi.org/10.2165/00023210-200317050-00004.
26. Rao, N. The Clinical Pharmacokinetics of Escitalopram. *Clin. Pharmacokinet.* **2007**, *46*, 281–290. https://doi.org/10.2165/00003088-200746040-00002.
27. Lv, J; Wang, Y.; Li, N. Oxidation of Citalopram with Sodium Hypochlorite and Chlorine Dioxide: Influencing Factors and NDMA Formation Kinetics. *Molecules* **2019**, *24*, 3065. https://doi.org/10.3390/molecules24173065.
28. Guo, Y.; Guo, Z.; Wang, J.; Ye, Z.; Zhang, L.; Niu, J. Photodegradation of three antidepressants in natural waters: Important roles of dissolved organic matter and nitrate. *Sci. Total Environ*. **2022**, *802*, 149825. https://doi.org/10.1016/j.scitotenv.2021.149825.
29. Jiménez-Holgado, C.; Calza, P.; Fabbri, D.; Dal Bello, F.; Medana, C.; Sakkas, V. Investigation of the Aquatic Photolytic and Photocatalytic Degradation of Citalopram. *Molecules* **2021**, *26*, 5331. https://doi.org/10.3390/molecules26175331.
30. Kwon, J-W.; Armbrust, K.L. Degradation of citalopram by simulated sunlight. *Environ. Toxicol. Chem.* **2005**, *24*, 1618–1623. https://doi.org/10.1897/04-522r.1.
31. Pinto, B.V.; Ferreira, A.P.G.; Cavalheiro, E.T.G. Thermal degradation mechanism for citalopram and escitalopram. *J. Therm. Anal. Calorim.* **2018**, *133*, 1509–1518. https://doi.org/10.1007/s10973-018-7226-7.
32. Frąckowiak, A.; Kamiński, B.; Urbaniak, B.; Dereziński, P.; Klupczyńska, A.; Darul-Duszkiewicz, M.; Kokot, Z.J. A study of ofloxacin and levofloxacin photostability in aqueous solutions. *J. Med. Sci.* **2016**, *85*, 238–244. https://doi.org/10.20883/jms.2016.178.
33. Arenas, M.; Martín, J.; Santis, J.L.; Aparicio, I.; Alonso, E. Enantioselective behavior of environmental chiral pollutants: A comprehensive review. *Cri. Rev. Environ. Sci. Technol.* **2022**, *52*, 2995–3034. https://doi.org/10.1080/10643389.2021.1900764.
34. Dhaneshwar, S.R.; Mahadik, M.V. Column Liquid Chromatography-Ultraviolet and Column Liquid Chromatography/Mass Spectrometry Evaluation of Stress Degradation Behavior of Escitalopram Oxalate. *J. AOAC Int.* **2009**, *92*, 138–147. https://doi.org/10.1093/jaoac/92.1.138.
35. Raman, B.; Sharma, B.A.; Ghugare, P.D.; Nandavadekar, S.; Singh, D.; Karmuse, P.K.; Kumar, A. Structural elucidation of process-related impurities in escitalopram by LC/ESI-MS and NMR. *J. Pham. Biomed. Anal*. **2010**, *53*, 895–901. https://doi.org/10.1016/j.jpba.2010.06.019.
36. Jiménez-Holgado, C.; Sakkas, V.; Richard, C. Phototransformation of Three Psychoactive Drugs in Presence of SedimentalWater Extractable Organic Matter. *Molecules* **2021**, *26*, 2466–2483. https://doi.org/10.3390/molecules26092466.
37. *Guideline ISO 5667-6:2014*; Water quality–Sampling–Part 6: Guidance on sampling of rivers and streams. Available online: https://www.iso.org/standard/55451.html (accessed on 7 September 2022)
38. *Guideline ISO 5667-4:2016*; Water quality–Sampling–Part 4: Guidance on sampling from lakes, natural and man-made. Available online: https://www.iso.org/standard/55451.html (accessed on 7 September 2022)
39. Surface Water: Nitrate Concentration, ARPAV. Available online: https://www.arpa.veneto.it/arpavinforma/indicatori-ambientali/indicatori_ambientali/idrosfera/qualita-dei-corpi-idrici/acque-superficiali-concentrazione-di-nitrati (accessed on 7 September 2022).
40. Manahan, S.E., Fundamentals of Aquatic Chemistry. In *Environmental Chemistry*, 8th ed.; Manahan, S.E., Ed.; CRC Press: NewYork, NY, USA, 2005; pp. 60-63.
41. Bro, R.; Smilde, A.K. Principal component analysis. *Anal. Methods* **2014**, *6*, 2812–2831. https://doi.org/10.1039/C3AY41907J.
42. Available online: https://database.ich.org/sites/default/files/Q2%28R1%29%20Guideline.pdf (accessed on 7 September 2022).
43. Hörsing, M.; Kosjek, T.; Andersen, H.R.; Heath, E.; Ledin, A. Fate of citalopram during water treatment with O_3, ClO_2, UV and fenton oxidation. *Chemosphere* **2012**, *89*, 129–135, http://dx.doi.org/10.1016/j.chemosphere.2012.05.024.
44. VEGA QSAR, ver. 1.2.0. Available online: https://www.vegahub.eu/portfolio-item/vega-qsar/ (accessed on 7 September 2022).
45. Toxicity Estimation Software Tool (T.E.S.T.), ver. 5.1.2. Available online: https://www.epa.gov/chemical-research/toxicity-estimation-software-tool-test (accessed on 7 September 2022).

46. Weininger, D.; Weininger, A.; Weininger, J.L. SMILES. 2. Algorithm for Generation of Unique SMILES Notation. *J. Chem. Inf. Comput. Sci.* **1989**, *29*, 97–101, https://doi.org/10.1021/ci00062a008.
47. Globally Harmonized System of Classification and Labelling of Chemicals (GHS). Available online: https://unece.org/sites/default/files/2021-09/GHS_Rev9E_0.pdf (accessed on 7 September 2022).